Analysis of shear viscosity and viscoelastic relaxation of liquid methanol based on molecular dynamics simulation and mode-coupling theory

Tsuyoshi Yamaguchi, and Antonio Faraone

Citation: The Journal of Chemical Physics **146**, 244506 (2017);
View online: https://doi.org/10.1063/1.4990408
View Table of Contents: http://aip.scitation.org/toc/jcp/146/24
Published by the American Institute of Physics

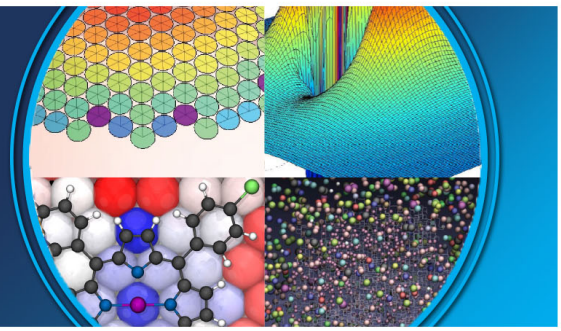

Analysis of shear viscosity and viscoelastic relaxation of liquid methanol based on molecular dynamics simulation and mode-coupling theory

Tsuyoshi Yamaguchi[1,a)] and Antonio Faraone[2]
[1]*Graduate School of Engineering, Nagoya University, Furo-cho B2-3 (611), Chikusa, Nagoya, Aichi 464-8603, Japan*
[2]*NIST Center for Neutron Research, National Institute of Standards and Technology, Gaithersburg, Maryland 20899, USA*

(Received 28 April 2017; accepted 12 June 2017; published online 30 June 2017)

The role of the prepeak structure of liquid methanol in determining its shear viscosity was studied by means of molecular dynamics (MD) simulation and mode-coupling theory (MCT). The autocorrelation function of the shear stress and the intermediate scattering functions at both the prepeak and the main peak were calculated from the MD trajectories. Their comparison based on MCT suggests that the viscoelastic relaxation in the ps regime is affected by the slow structural dynamics at the prepeak. On the other hand, the MCT for molecular liquids based on the interaction-site model (site-site MCT) fails to describe the coupling between the prepeak dynamics and shear stress. The direct evaluation of the coupling between the two-body density and the shear stress reveals that the viscoelastic relaxation is actually affected by the prepeak dynamics, although the coupling is not captured by the site-site MCT. The site-site MCT works well for a model methanol without partial charges, suggesting that the failure of the site-site MCT originates from the existence of a hydrogen-bonding network structure. *Published by AIP Publishing.* [http://dx.doi.org/10.1063/1.4990408]

I. INTRODUCTION

1-alcohol is a class of amphiphilic molecules in which a polar OH group is attached to an end of a nonpolar linear alkyl chain. In its liquid phase, the OH groups form the characteristic linear hydrogen-bonding network structure. The polar OH groups cluster together through the hydrogen bonding, and the excluded alkyl chains also gather. The domain structure of 1-alcohols composed of the polar and nonpolar domains resembles that of room-temperature ionic liquids and surfactant solutions, and it is an interesting question how such a structure affects the macroscopic properties of liquid alcohols. In particular, since the characteristic mesoscopic structure of surfactant solutions is responsible for the large structural viscosity, the effects on shear viscosity could be especially important also in the case of 1-alcohols.

The hydrogen-bonding network of 1-alcohols appears in the reciprocal space as a prepeak in the scattering experiments. The prepeak of 1-alcohols appears as a distinct peak when the alkyl chain is longer than ethyl,[1–4] and the prepeak shifts to lower wavenumber with increasing the chain length, as is the case of room-temperature ionic liquids.[5–8]

The dynamics of the network structure can be probed through QuasiElastic Neutron Scattering (QENS) at the prepeak. Sillrén and co-workers measured the intermediate scattering function of 1-propanol at the pre- and the main peaks by means of neutron spin echo (NSE) spectroscopy and found that the dynamics at the prepeak is slower than that at the main peak.[9] The slower dynamics of the prepeak has also been reported for room-temperature ionic liquids.[10]

One of us (TY) studied very recently the structural dynamics and viscoelastic relaxation of a series of 1-alcohols from 1-butanol to 1-dodecanol by molecular dynamics (MD) simulation.[11] Slower relaxation of the intermediate scattering function at the prepeak was confirmed by the simulation. The viscoelastic relaxation of these 1-alcohols was bimodal. Comparing with the intermediate scattering functions, the faster and the slower modes of the viscoelastic relaxation were ascribed to the structural dynamics at the main peak and the prepeak, respectively.

Methanol is the simplest 1-alcohol composed of one methyl and one OH groups. One of us (AF) studied its structure and dynamics by means of neutron quasielastic spectroscopy with isotopic substitution.[12,13] The static structure factor of methanol shows a broad prepeak at $q = 12\ \mathrm{nm}^{-1}$, which overlaps with the main peak at $q = 17\ \mathrm{nm}^{-1}$. The analysis based on the isotope substitution and MD simulation demonstrates that the prepeak can be assigned to the OH group correlation, while the contribution of the methyl group is dominant at the main peak. The quasielastic scattering revealed that the dynamics at the prepeak is slower than that at the main peak, as in the case of longer 1-alcohols.[9,11]

In this work, the relationship between the structural dynamics and the viscoelastic relaxation of methanol is investigated in detail based on the mode-coupling theory (MCT), in order to clarify whether the dynamics of the network structure of methanol also contributes to the shear viscosity of methanol. Calculations on a hypothetical model of methanol without partial charges are also performed in order to extract the effects of the hydrogen-bonding network. The comparison between the time profiles of the viscoelastic relaxation and the intermediate scattering functions is performed first, as

a)E-mail: yamaguchi.tsuyoshi@material.nagoya-u.ac.jp

we have done on higher alcohols.[11] The time profiles suggest the contribution of the dynamics at the prepeak to the slowest mode of the viscoelastic relaxation. The calculation based on the MCT for molecular liquids of interaction-site description (site-site MCT) is applied for detailed analysis.[14,15] However, the site-site MCT hardly exhibits the coupling between the shear stress and the prepeak structure, and it fails to reproduce the slowest mode of the viscoelastic relaxation. The cross correlation between the shear stress and the two-body density is calculated directly from MD simulation in order to resolve the origin of the apparent contradiction. The analysis of the cross correlation demonstrates that the coupling between the shear stress and the prepeak structure does indeed exist, though it is lost during the approximation employed in the site-site MCT.

II. THEORY

The Kubo-Green theory states that the steady-state shear viscosity of liquids, η_0, is given by the time correlation function of shear stress, $\mathbf{P}^{(s)}$, as[16–18]

$$\eta_0 = \int_0^\infty G(t)\, dt, \tag{1}$$

$$G(t) \equiv \frac{V}{k_B T} \left\langle P_{xz}^{(s)} e^{iLt} P_{xz}^{(s)} \right\rangle, \tag{2}$$

where k_B, T, and V mean the Boltzmann constant, the absolute temperature, and the volume of the system, respectively, and L stands for the Liouvillian operator.

The site-site MCT approximates the time correlation function of the shear stress, Eq. (2), in terms of the partial intermediate scattering function as[14,15]

$$G(t) = \frac{k_B T}{60\pi^2} \int_0^\infty dq\, q^4 Tr \left[\left\{ \frac{d\mathbf{c}(q)}{dq} \cdot \mathbf{F}(q,t) \right\}^2 \right], \tag{3}$$

where bold symbols are matrices with indices of interaction sites, and a dot "·" stands for the product of two matrices. The partial intermediate scattering function, $F_{\alpha\gamma}(q,t)$, is defined by[19]

$$F_{\alpha\gamma}(|\mathbf{q}|,t) \equiv \frac{1}{V} \left\langle \rho_\alpha^*(\mathbf{q})\, e^{iLt} \rho_\gamma(\mathbf{q}) \right\rangle, \tag{4}$$

where $\rho_\alpha(\mathbf{q})$ stands for the density field of the site α at the wavevector $\mathbf{q}$. The initial value of $F_{\alpha\gamma}(q,t)$,

$$\chi_{\alpha\gamma}(q) \equiv F_{\alpha\gamma}(q, t=0), \tag{5}$$

is called the partial static structure factor. The direct correlation function, $\mathbf{c}(q)$ in Eq. (3), is related to the partial static structure factor as

$$\mathbf{c}(q) \equiv \left[\boldsymbol{\rho} \cdot \boldsymbol{\omega}(q)\right]^{-1} - \boldsymbol{\chi}^{-1}(q), \tag{6}$$

where the matrix $\boldsymbol{\rho}$ is defined as $\rho_{\alpha\gamma} = \rho_\alpha \delta_{\alpha\gamma}$, and ρ_α stands for the number density of the site α. The intramolecular correlation function, $\omega_{\alpha\gamma}(q)$, is defined as

$$\omega_{\alpha\gamma}(|\mathbf{q}|) \equiv \left\langle \rho_{s,\alpha}^*(\mathbf{q})\, \rho_{s,\gamma}(\mathbf{q}) \right\rangle, \tag{7}$$

where $\rho_{s,\alpha}(\mathbf{q})$ stands for the density field of the site α within a tagged molecule at the wavevector $\mathbf{q}$.

The site-site Ornstein-Zernike (SSOZ) equation, Eq. (6), is a definition of $\mathbf{c}(q)$ in terms of $\boldsymbol{\chi}(q)$ and $\boldsymbol{\omega}(q)$. Combined with closure equations such as the hypernetted-chain (HNC) or the Kovalenko-Hirata (KH) ones, it can yield the static structure factor of molecular liquids analytically from intermolecular interactions.[19] In this work, however, the SSOZ equation is used merely to calculate $\mathbf{c}(q)$ from $\boldsymbol{\chi}(q)$ obtained by the MD simulation.

The MCT approximation can also be applied to the memory function for the partial intermediate scattering functions. The liquid dynamics and the shear viscosity are then calculated from the static structure in a self-consistent way.[20] Since the purpose of this work is to relate the shear viscosity with the structural dynamics, however, the partial intermediate scattering functions are evaluated by the MD simulation instead of the self-consistent MCT calculation in order to avoid the effects of unnecessary errors associated with the evaluation of the partial intermediate scattering functions.

Equations (1)–(3) are combined and transformed as

$$\eta_0 = \int_0^\infty \kappa_\eta(q)\, dq, \tag{8}$$

$$\kappa_\eta(q) \equiv \frac{k_B T q^4}{60\pi^2} \int_0^\infty dt\, Tr \left[\left\{ \frac{d\mathbf{c}(q)}{dq} \cdot \mathbf{F}(q,t) \right\}^2 \right]. \tag{9}$$

The steady-state shear viscosity is divided into the contributions of liquid dynamics at various wavenumbers in Eq. (8), and the contribution is described by $\kappa_\eta(q)$ in Eq. (9) within the site-site MCT approximation.

Under the assumptions that the integral over q in Eq. (3) is dominated by the contribution around q^*, and that the time profile of the intermediate scattering function at q^* scarcely depends on the atomic indices, the time profile of $G(t)$ in Eq. (3) is determined by $I^2(q^*,t)$,[21,22] where $I(q,t)$ is a linear combination of the partial intermediate scattering function as

$$I(q,t) \equiv \sum_{\alpha\gamma} B_{\alpha\gamma} F_{\alpha\gamma}(q,t). \tag{10}$$

Here, $B_{\alpha\gamma}$ can be taken arbitrarily under the assumption that the structural dynamics depends little on the atomic indices. In particular, by choosing $B_{\alpha\gamma} = b_\alpha b_\gamma$, where b_α stands for the neutron or the X-ray scattering length of the atom α, $I(q,t)$ is equivalent to the intermediate scattering functions determined by quasielastic scattering experiments. Since $G(t)$ is also accessible with rheological experiments, the experimental comparison between $G(t)$ and $I^2(q^*,t)$ gives information on the contribution of the liquid structure around q^* to shear viscosity. The characteristic wavenumber q^* is usually taken to be the peak positions of the prepeak or the main peak in such comparisons.[21,22]

The MCT expression of the shear viscosity can be derived through the projection operator formalism. The two-body density in the reciprocal space is defined as

$$\rho_{\alpha\gamma}^{(2)}(\mathbf{q}) \equiv \rho_\alpha^*(\mathbf{q})\, \rho_\gamma(\mathbf{q}), \tag{11}$$

$$\delta\rho_{\alpha\gamma}^{(2)}(\mathbf{q}) \equiv \rho_{\alpha\gamma}^{(2)}(\mathbf{q}) - \left\langle \rho_{\alpha\gamma}^{(2)}(\mathbf{q}) \right\rangle. \tag{12}$$

Since the statistical average of $\rho_{\alpha\gamma}{}^{(2)}(\mathbf{q})$ is proportional to the partial static structure factor, $\chi_{\alpha\gamma}(q)$, $\rho_{\alpha\gamma}{}^{(2)}(\mathbf{q})$ can be regarded as the instantaneous liquid structure. The projection operators onto the vector space spanned by $\{\delta\rho_{\alpha\gamma}{}^{(2)}(\mathbf{q})\}$, denoted as $P^{(2)}$, are inserted into the both sides of the time propagation operator, e^{iLt}, as

$$G(t) \cong \frac{V}{k_B T}\left\langle P_{xz}^{(s)} P^{(2)} e^{iLt} P^{(2)} P_{xz}^{(s)}\right\rangle. \tag{13}$$

The factorization approximation is applied here as

$$\begin{aligned}&\left\langle \delta\rho_{\alpha\gamma}^{(2)*}(\mathbf{q})\, e^{iLt}\delta\rho_{\alpha'\gamma'}^{(2)}(\mathbf{q}')\right\rangle \\ &\quad\cong 8\pi^3 V\left[F_{\alpha\alpha'}(q,t)\,F_{\gamma\gamma'}(q,t)\,\delta(\mathbf{q}-\mathbf{q}')\right. \\ &\qquad\left. + F_{\gamma\alpha'}(q,t)\,F_{\alpha\gamma'}(q,t)\,\delta(\mathbf{q}+\mathbf{q}')\right],\end{aligned} \tag{14}$$

which assumes the Gaussian statistics of $\{\rho_\alpha(\mathbf{q})\}$, and the MCT expression of $G(t)$ is given by

$$\begin{aligned}G(t) \cong \frac{k_B T}{16\pi^3}\int d\mathbf{q}\sum_{\alpha\alpha'\gamma\gamma'}&\left[V_{\eta,\alpha\gamma}(\mathbf{q})\,F_{\alpha\alpha'}(q,t)\right. \\ &\left.\times F_{\gamma\gamma'}(q,t)\,V_{\eta,\alpha'\gamma'}(\mathbf{q})\right].\end{aligned} \tag{15}$$

The function $V_{\eta,\alpha\gamma}(\mathbf{q})$, which is called "vertex function," is defined as

$$\begin{aligned}V_{\eta,\alpha\gamma}(\mathbf{q}) = \frac{16\pi^3 V}{k_B T}\int d\mathbf{q}'\sum_{\alpha'\gamma'}&\left\langle \delta\rho_{\alpha\gamma}^{(2)*}(\mathbf{q})\,\delta\rho_{\alpha\gamma}^{(2)}(\mathbf{q}')\right\rangle^{-1} \\ &\times\left\langle \delta\rho_{\alpha\gamma}^{(2)}(\mathbf{q}')\,P_{xz}^{(s)}\right\rangle.\end{aligned} \tag{16}$$

It describes the strength of the coupling between the shear stress and the two-body density. The site-site MCT given by Eq. (3) approximates the vertex function as

$$V_{\eta,\alpha\gamma}(\mathbf{q}) \cong \frac{q_x q_z}{q}\frac{dc_{\alpha\gamma}(q)}{dq}. \tag{17}$$

One can derive the MCT expression for the memory function of the intermediate scattering functions at finite wavenumbers in a similar way with the projection to the two-body density and the application of the factorization approximation. In the case of the memory function at finite wavenumbers, there is an additional approximation that the projected Liouvillian operator is replaced with the ordinary one. On the other hand, since $G(t)$ corresponds to the memory function of the transverse current *in the long-wavelength limit*, the replacement of the Liouvillian operator is performed at the derivation of the Kubo-Green formula, Eqs. (1) and (2), without any approximation.[18]

Instead of Eq. (13), the projection operator is inserted in this work into only one side of the time propagation operator as

$$G(t) \cong \frac{V}{k_B T}\left\langle P_{xz}^{(s)} P^{(2)} e^{iLt} P_{xz}^{(s)}\right\rangle, \tag{18}$$

which can be transformed as

$$G(t) \cong \int d\mathbf{q}\sum_{\alpha\gamma}\frac{q_x q_z}{q^2}\left[V_{\eta,\alpha\gamma}(\mathbf{q})\,\rho_{\eta,\alpha\gamma}^{(2)}(q,t)\right], \tag{19}$$

$$\rho_{\eta,\alpha\gamma}^{(2)}(q,t) \equiv \frac{q^2}{q_x q_z}\left\langle \delta\rho_{\alpha\gamma}^{(2)}(\mathbf{q})\, e^{iLt} P_{xz}^{(s)}\right\rangle. \tag{20}$$

The trivial orientational dependence is factored out in the definition of $\rho_{\eta,\alpha\gamma}{}^{(2)}(q,t)$, Eq. (20), as a scalar function. The function $\rho_{\eta,\alpha\gamma}{}^{(2)}(q,t)/k_B T$ is interpreted as the response of the two-body density according to the linear response theory. It is in principle observable by means of experiments such as Rheo-SANS,[23] which measures the small-angle neutron scattering (SANS) under the sheared condition, although the q-range in question is higher than that of SANS in this work.

The physical interpretation of Eq. (19) is then quite simple. The liquid structure is distorted by the applied shear flow, which is described by $\rho_{\eta,\alpha\gamma}{}^{(2)}(q,t)$. Due to the coupling between the liquid structure and the shear stress, which is described by the vertex function, the distorted liquid structure yields the shear stress, which is observed as the response of the shear stress to the applied shear flow. One of us (TY) has applied similar theoretical formulation to self-diffusion, ultrasonic absorption, and electrical conductivity.[24–27]

The pure-shear deformation can be described as the superposition of the uniaxial compression and the uniaxial expansion, where the axes of the compression and the expansion are orthogonal to each other. The sign of $\rho_{\eta,\alpha\gamma}{}^{(2)}(q,t)$ is so defined that it has the same sign as the structural response along the compression axis.

Under the approximations employed in the site-site MCT, the response of the two-body density is given by

$$\rho_{\eta,\alpha\gamma}^{(2)}(q,t) \cong -k_B T q\left[\mathbf{F}(q,t)\cdot\frac{d\mathbf{c}(q)}{dq}\cdot\mathbf{F}(q,t)\right]_{\alpha\gamma}. \tag{21}$$

The comparison between Eq. (21) and $\rho_{\eta,\alpha\gamma}{}^{(2)}(q,t)$ evaluated directly through the MD simulation can be a test for the approximation involved in the site-site MCT.

III. MD SIMULATION

The MD simulation of liquid methanol was performed at 290 K and 1 atm in almost the same way as one of us (AF) performed in the previous works.[12,13] GROMACS 5.1.2 package was used for calculation.[28,29] The system was composed of 2048 methanol molecules, which were described by the OPLS-AA model.[30] The molecules were enclosed in a cubic cell, to which periodic boundary condition was applied. The equilibrated structure was taken from the previous work.[13] The equation of motion was integrated by the leap-frog algorithm with the time step of 2 fs. The production run of 5 ns length was used in most calculations. Since the statistics of the cross correlation between the shear stress and the two-body density, Eq. (20), was low, the production run was lengthened up to 50 ns for this correlation function. The Nosé-Hoover thermostat[31] and the Parrinello-Rahman barostat were employed to realize the NPT ensemble. The long-range part of the Coulombic interaction was handled with the particle-mesh-Ewald method with the Fourier spacing of 0.12 nm. The short-range part of the interactions was cut off at 1.1 nm. The length of the intramolecular bonds associated with the hydrogen atoms was fixed with the LINCS algorithm,[32] and the other bond lengths and bond angles were treated as flexible. All the five components of the shear stress tensor were utilized for the calculation of the correlation functions associated with the shear stress tensor under the consideration of the trivial orientational symmetry, although the definitions were given with only the xz-component. The shear stress tensor was calculated

at every 2 steps and recorded at every 100 steps. The spatial coordinates were recorded at every 100 steps. The q-dependent correlation functions were calculated directly in the reciprocal space. Although the absolute values of the lattice vectors fluctuated during the production runs in the NPT ensemble, the magnitude of the fluctuation was rather small owing to the small compressibility, and the average value was used to show the correlation functions.

In order to examine the effects of the hydrogen-bonding network on the shear viscosity of methanol in detail, we also performed the MD simulation with a model methanol without hydrogen bonding, hereafter called the non-HB methanol, as was performed in the previous work.[12] The partial charges on all the sites were removed in the model, while other intra- and intermolecular interactions were kept the same. The NVT ensemble was employed for the non-HB methanol in order to avoid the vaporization, and the value of the density was set to the average value obtained from the MD simulation of the normal methanol. The equilibration run of 5 ns length was performed first, starting from the equilibrium configuration of the normal methanol, and the subsequent production runs of 5 ns and 50 ns were performed.

IV. RESULTS AND DISCUSSION

Figure 1 shows the partial intermediate scattering functions, $F_{\alpha\gamma}(q,t)$, at four different times, t = 0, 0.2, 1, and 4 ps, which are calculated by our MD simulation. Only the self-correlations of the O-, H-, and C-atoms are plotted, where the H-atom stands for the hydrogen atom of the OH group, and the three hydrogen atoms in the methyl group were referred to as "M," as was performed in the previous work.[13]

The static structure factor, $\boldsymbol{\chi}(q) = \mathbf{F}(q,t = 0)$, shows two peaks at q = 12 nm^{-1} and 17 nm^{-1}, which corresponds to the pre- and the main peaks, respectively. The main peak is principally assigned to the correlation of the C-atom, while the prepeak is to those of the O- and the H-atoms, as was demonstrated in the previous work.[13]

The decay rates of the O- and the H-components at the prepeak are close to each other, and they are slower than that of the C-atom at the main peak. The relaxation at the prepeak is slower than at the main peak, in harmony with the previous work.[13]

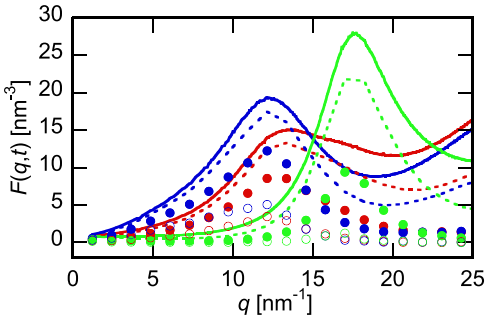

FIG. 1. The O–O (red), H–H (blue), and C–C (green) components of the partial intermediate scattering functions, $F(q,t)$, of the normal methanol from MD simulation are plotted as the functions of wavenumber, q. The functions at the initial time, which are equal to the partial static structure factors, $\chi(q)$, are shown with the solid curves, while those at t = 0.2 ps, 1 ps, and 4 ps are with the dashed curves, filled circles, and open circles, respectively.

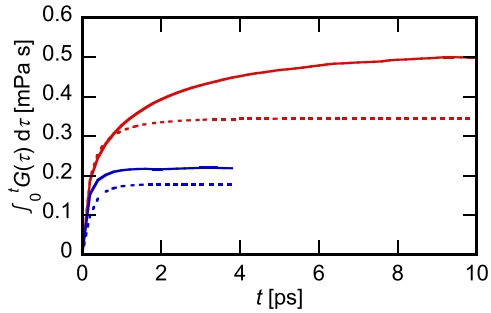

FIG. 2. The running integrals of $G(\tau)$ of the normal (red) and the non-HB (blue) methanols from 0 to t evaluated from the MD simulation (solid) and those calculated with the site-site MCT (dashed).

The running integral of $G(t)$ from the MD simulation is shown in Fig. 2 as the red solid curve. The steady state shear viscosity, η_0, which corresponds to the long-time limiting value of the running integral, is 0.51 mPa s, which is close to the experimental value, 0.59 mPa s.[33]

The normalized running integral of $G(t)$ was compared with those of $I^2(q,t)$ at the two peaks in Fig. 3. The coefficients in Eq. (10) are taken to be $B_{\alpha\gamma} = b_\alpha b_\gamma$, where b_α stands for the coherent scattering length of the corresponding atom α of methanol-d_4 in this work to imitate the intermediate scattering function of methanol-d_4 determined by QENS spectroscopy.[13] The values of the running integral of $I^2(q,t)$ may be overestimated a little due to the numerical integration with the interval of Δt = 0.2 ps.

The convergence of the running integral at the prepeak is slower than that at the main peak, as was expected from the intermediate scattering function. Comparing the dynamics of the shear stress with that of the intermediate scattering function, the former exhibits the broader distribution of relaxation times. The slowest part of the relaxation appears to be as slow as $I^2(q,t)$ at the prepeak. The time profiles in Fig. 3 thus suggest that the shear viscosity of liquid methanol is affected by the dynamics of both peaks as are the cases of higher alcohols in the previous work.[11] Although $G(t)$ of methanol does not appear bimodal as the higher alcohols do, this is ascribed to the small separation of the time scales of the dynamics at the two peaks.

The site-site MCT expression of $G(t)$, Eq. (3), is applied to methanol, and the result is compared with that from the MD

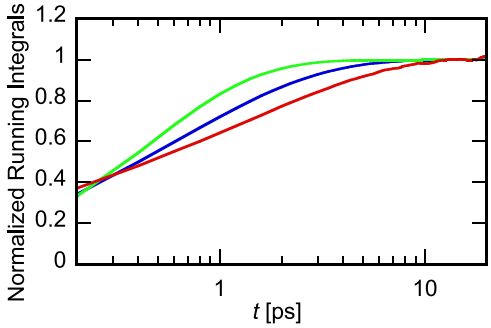

FIG. 3. The normalized running integral of $G(\tau)$ of the normal methanol from 0 to t (red) is compared with the corresponding normalized running integrals of $I^2(q,\tau)$ at the prepeak (q = 12.1 nm^{-1}, blue) and the main peak (q = 17.0 nm^{-1}, green).

simulation in Fig. 2. The methanol molecule is regarded as the three-site model in the MCT calculation, in order to avoid the strong low-q singularity of $\chi^{-1}(q)$ in the calculation of the direct correlation function through Eq. (6). The introduction of the three-site picture corresponds to the restriction of the vector space onto which the projection operator $P^{(2)}$ is applied. We consider that the effects of the three-site approximation are marginal, because the slow dynamics of the M-atoms will follow that of the C-atom. The integral over q was truncated at $q = 32$ nm^{-1}. Although the truncation may result in the underestimation of the short-time part, it does not affect the slow dynamics under interest. Both the direct correlation function and the intermediate scattering function are determined from the same MD trajectory. The difference between the two time-correlation functions is thus ascribed to the limitation of the site-site MCT approximation.

As shown in Fig. 2, the site-site MCT underestimates the steady-state shear viscosity. The relaxation of $G(t)$ of the site-site MCT is faster than that of the MD simulation, and it is as fast as $I^2(q,t)$ at the main peak shown in Fig. 3. Therefore, the time profile in Fig. 2 suggests the decoupling between the shear stress and the hydrogen-bonding network structure.

The decoupling also appears in the wavenumber profile of $\kappa_\eta(q)$ plotted in Fig. 4. The shear viscosity originates mainly from the structure at the main peak region, $q > 15$ nm^{-1}, and no structure is observed in the prepeak region.

Given the decoupling between the shear stress and the prepeak structure in the site-site MCT, it is necessary to revisit the tentative assignment of the slowest mode of the shear relaxation observed in Fig. 3 to the relaxation of $I^2(q,t)$ at the prepeak. We therefore examine their coupling in detail based on the cross correlation between the two-body density and the shear stress, $\rho_{\eta,\alpha\gamma}{}^{(2)}(q,t)$.

The cross-correlation functions at three different times, t = 0, 0.2, and 1 ps, are plotted in Figs. 5(a)–5(c). The functions determined directly from the MD simulation are shown with dots, while those from the site-site MCT approximation, Eq. (21), are with solid lines.

The initial profiles of the cross-correlation functions are reproduced qualitatively by Eq. (21), although a small discrepancy is found [Fig. 5(a)]. The difference increases at the end of the binary collision, t = 0.2 ps [Fig. 5(b)]. In particular, the theory underestimates the coupling with the O–O correlation at the prepeak, while that with the C–C correlation at the main peak is overestimated. At t = 1 ps when $I^2(q,t)$ at the main peak has almost decayed, the remaining coupling with the prepeak structure is much larger in the MD profile than in the theoretical one [Fig. 5(c)]. The time profile of $\rho_{\eta,\alpha\gamma}{}^{(2)}(q,t)$ was integrated from t = 0 to 20 ps in Fig. 5(d). The integrated strength of the coupling with the prepeak is greatly underestimated by the theory, while that with the main peak is a little overestimated. The weak coupling with the prepeak structure by the MCT-like approximation, Eq. (21), thus explains the apparent decoupling between the shear stress and the prepeak structure in the site-site MCT.

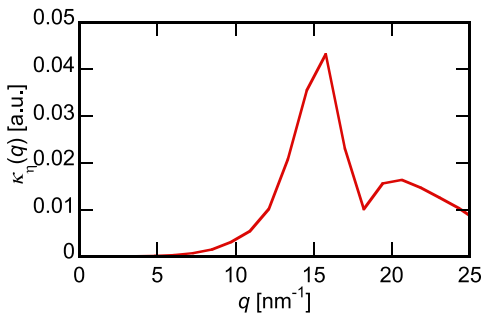

FIG. 4. The wavenumber profile of the contribution of the liquid structure at q to the steady-state shear viscosity η_0 in the site-site MCT, $\kappa_\eta(q,t)$, defined by Eq. (9).

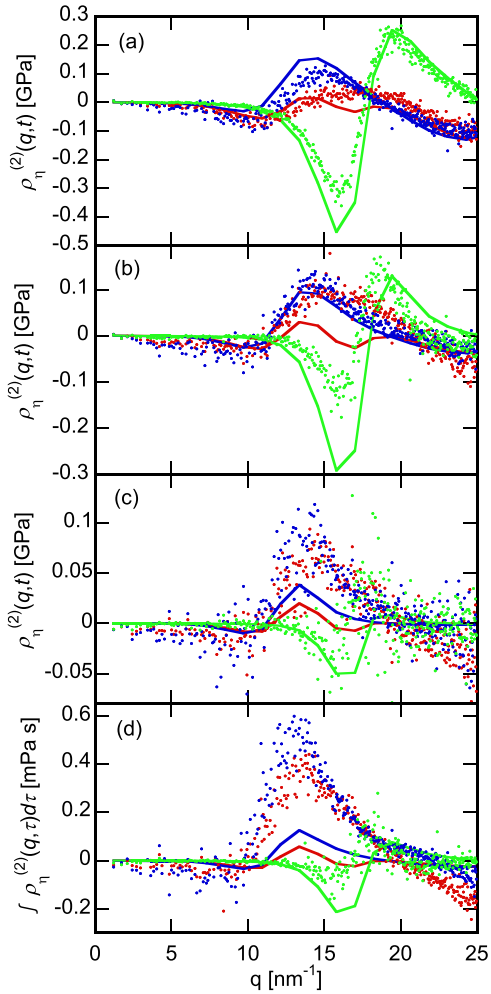

FIG. 5. The cross-correlation function between the two-body density and the shear stress, $\rho_{\eta,\alpha\gamma}{}^{(2)}(q,t)$, of the normal methanol at t = 0, 0.2 ps, and 1 ps is shown in panels (a)–(c), respectively, and its time integral from t = 0 to 20 ps is in panel (d). The O–O, H–H, and C–C components are plotted with red, blue, and green. The dots are those determined from the MD simulation, while the site-site MCT approximations are drawn with solid curves.

The initial profile of $\rho_{\eta,\mathrm{CC}}{}^{(2)}(q,t)$ is negative and positive on the low-q and high-q sides of the main peak of $\chi_{\mathrm{CC}}(q)$, respectively. The main peak of the C–C correlation thus shifts to the higher-q along the compression axis, reflecting the decrease in the interatomic distance upon compression. The time profile of $\rho_{\eta,\mathrm{CC}}{}^{(2)}(q,t)$ indicates that the shifted C–C correlation relaxes to the equilibrium one in a monotonic way.

The positive response of the prepeak in $\rho_{\eta,\mathrm{OO}}{}^{(2)}(q,t)$ and $\rho_{\eta,\mathrm{HH}}{}^{(2)}(q,t)$ means that the hydrogen-bonding chain of methanol aligns along the expansion axis, and the

relaxation of the alignment is controlled by the dynamics of the intermediate scattering function at the prepeak. It is this alignment that the site-site MCT fails to describe.

The slowest part of $G(t)$ in Fig. 2 is assigned to the coupling with the prepeak structure based on the analysis of $\rho_{\eta,\alpha\gamma}{}^{(2)}(q,t)$, which validates the MCT approximation that the slow dynamics of the shear stress is described in terms of the bilinear product of the partial intermediate scattering functions. The weak coupling between the shear stress and the prepeak structure is thus ascribed to the failure of the description of the vertex function in the site-site MCT. On the other hand, the qualitative agreement at $t = 0$ exhibited in Fig. 5(a) suggests that the vertex function of the site-site MCT works fairly well at the initial time. Given that the discrepancy between the simulation and the theory is evident at $t = 0.2$ ps, we consider that the failure of the vertex function in the long-time region results from the short-time non-Gaussian dynamics.

Figure 6 shows the partial static structure factors of the non-HB methanol from MD simulation. The structure of the normal methanol is also plotted for comparison. The prepeak completely disappears in the non-HB methanol, reflecting the absence of the network structure. The C–C correlation is little affected by the hydrogen-bonding because it is mainly determined by repulsive packing. The peak position of the O–O correlation is the same as the C–C correlation in the case of the non-HB methanol. The height of the former is lower than that of the latter due to the smaller size of the O-atom than the methyl group.

The running integral of $G(t)$ of the non-HB methanol is shown in Fig. 2 as the blue solid curve. The value of the steady-state shear viscosity is much reduced, and the relaxation of the shear stress becomes much faster compared with that of normal methanol.

The calculation of $G(t)$ using the site-site MCT is also performed on the non-HB methanol, and the result is shown as the blue dashed curve in Fig. 2. The site-site MCT describes the time profile of $G(t)$ well. The small underestimation of η_0 is explained by the smaller contribution of the binary collision, which is ascribed to the high-q cutoff in the q-integral of Eq. (3).

The response of the two-body density of the non-HB methanol, $\rho_{\eta,\alpha\gamma}{}^{(2)}(q,t)$, is shown in Fig. 7. At initial time, $t = 0$, the shapes of the responses of all the components are

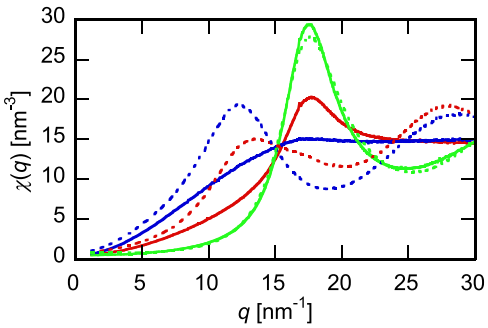

FIG. 6. The partial static structure factors of the normal (dashed) and the non-HB (solid) methanols, both of which are calculated from MD simulation. The O–O, H–H, and C–C components are plotted with red, blue, and green, respectively.

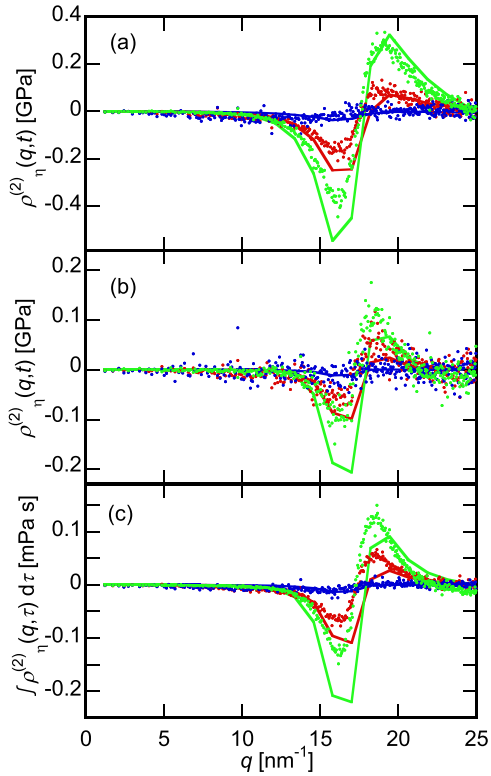

FIG. 7. The cross-correlation function between the two-body density and the shear stress, $\rho_{\eta,\alpha\gamma}{}^{(2)}(q,t)$, of the non-HB methanol at $t = 0$ and 0.4 ps is shown in panels (a) and (b), respectively, and its time integral from $t = 0$ to 2 ps is in panel (c). The O–O, H–H, and C–C components are plotted with red, blue, and green. The circles are those determined from the MD simulation, while the site-site MCT approximations are drawn with solid curves.

similar to one another, and they also resemble $\rho_{\eta,\mathrm{CC}}{}^{(2)}(q,t = 0)$ of the normal methanol shown in Fig. 5(a). The difference in the amplitudes among the atomic components originates in that of the peak height of the static structure factor in Fig. 6. The peaks of all the components shift to higher-q along the compression axis as is expected. The profiles at the initial time are reproduced by the site-site MCT fairly well.

At $t = 0.4$ ps, the amplitudes of $\rho_{\eta,\alpha\gamma}{}^{(2)}(q,t)$s decay with keeping their shapes as are shown in Fig. 7(b). Comparing the profiles from the MD simulation and the site-site MCT, the latter overestimates the decay of the negative peaks at $q = 16$ nm^{-1}, while it underestimates that of the positive peaks at $q = 19$ nm^{-1}. The decay rates of the two profiles agree with each other on average, which explains the agreement of the time profiles of $G(t)$ exhibited in Fig. 2.

The integrated responses are shown in Fig. 7(c). The negative peak at $q = 16$ nm^{-1} is overestimated and the positive one at $q = 19$ nm^{-1} is underestimated due to the difference in the decay rates demonstrated in Fig. 7(b). However, the magnitude of the response of the two-body density is reproduced fairly well by the site-site MCT.

The site-site MCT describes the response of the two-body density of the non-HB methanol, while it fails on that of the prepeak structure of the normal methanol. The failure of the site-site MCT on the shear viscosity of the normal methanol is thus ascribed to the hydrogen-bonding network structure.

There are other classes of liquids and solutions that exhibit prepeak structures, and the roles of the prepeak in dynamic properties of these systems have been investigated both theoretically and experimentally.

One example is room-temperature ionic liquid with long alkyl chains. One of us (TY) applied the self-consistent site-site MCT to model ionic liquids and found the presence of the direct coupling between the shear stress and the structural dynamics at the prepeak.[34] However, such a direct coupling was not so evident in experiments.[21,22,34]

Another example is the solutions of colloidal particles with both sticky attraction and long-range repulsion. The glass transition of these colloidal systems was investigated in detail both by computer simulations and the self-consistent MCT calculations.[35,36] The long-range repulsive interaction leads to the formation of the mesoscopic structure represented as the prepeak, and the structural relaxation at the prepeak is the slowest microscopic dynamics. However, Henrich and co-workers have shown by the self-consistent MCT calculation that the presence of the prepeak does not affect the nature of the glass transition, that is, the slow structural relaxation at the prepeak scarcely affects the microscopic dynamics.[36] Their result is consistent with that of ionic liquid in Ref. 34 in that the slow structural relaxation at the prepeak does not appear in the memory function of the intermediate scattering function at the main peak. The time correlation function of the shear stress was not evaluated in these studies, and it would be interesting to know whether the prepeak dynamics of the colloidal solutions contribute to their viscoelastic relaxation.

V. SUMMARY

The viscoelastic relaxation of liquid methanol was calculated by MD simulation and compared with the dynamics of the liquid structure at the prepeak and the main peak. The time-profile based comparison suggested the coupling between the shear stress and the prepeak structure. Although the coupling was not described by the site-site MCT, it was confirmed by the analysis based on the cross-correlation function between the shear stress and the two-body density. It was thus revealed that the shear viscosity of liquid methanol is affected by the dynamics of the hydrogen-bonding network structure, as in the case of higher alcohols. The apparent decoupling in the site-site MCT calculation was ascribed to the insufficient approximation of the vertex function in the long-time region, which may result from the non-Gaussian short-time dynamics, which is, in turn, due to the presence of the hydrogen-bonding network structure.

ACKNOWLEDGMENTS

We are grateful to Dr. C. E. Bertrand for the use of the parameter files for GROMACS and the equilibrated configurations. This work was supported by the Japan Society for the Promotion of Science (JSPS), KAKENHI Grant No. 16K05514.

[1] M. Tomšič, M. Bešter-Rogač, A. Jamnik, W. Kunz, D. Touraud, A. Bergmann, and O. Glatter, J. Phys. Chem. B **108**, 7021 (2004).
[2] M. Tomšič, A. Jamnik, G. Fritz-Popovski, O. Glatter, and L. Vlček, J. Phys. Chem. B **111**, 1738 (2007).
[3] R. Böhmer, C. Gainaru, and R. Richert, Phys. Rep. **545**, 125 (2014).
[4] A. Perera, Phys. Chem. Chem. Phys. **19**, 1062 (2017).
[5] J. N. A. C. Lopes and A. A. H. Pádua, J. Phys. Chem. B **110**, 3330 (2006).
[6] O. Russina and A. Triolo, Faraday Discuss. **154**, 97 (2012).
[7] K. Fujii, R. Kanzaki, T. Takamuku, Y. Kameda, S. Kohara, M. Kanakubo, M. Shibayama, S. Ishiguro, and Y. Umebayashi, J. Chem. Phys. **135**, 244502 (2011).
[8] K. Shimizu, C. E. S. Bernardes, and J. N. C. Lopes, J. Phys. Chem. B **118**, 567 (2014).
[9] P. Sillrén, A. Matic, M. Karlsson, M. Koza, M. Maccarini, P. Fouquet, M. Götz, Th. Bauer, R. Gulich, P. Lunkenheimer, A. Loidl, J. Mattsson, C. Gainaru, E. Vynokur, S. Schildmann, S. Bauer, and R. Böhmer, J. Chem. Phys. **140**, 124501 (2014).
[10] M. Kofu, M. Nagao, T. Ueki, Y. Kitazawa, Y. Nakamura, S. Sawamura, M. Watanabe, and O. Yamamuro, J. Phys. Chem. B **117**, 2773 (2013).
[11] T. Yamaguchi, J. Chem. Phys. **146**, 094511 (2017).
[12] C. E. Bertrand, J. L. Self, J. R. D. Copley, and A. Faraone, J. Chem. Phys. **145**, 014502 (2016).
[13] C. E. Bertrand, J. L. Self, J. R. D. Copley, and A. Faraone, J. Chem. Phys. **146**, 194501 (2017).
[14] T. Yamaguchi and F. Hirata, J. Chem. Phys. **115**, 9340 (2001).
[15] T. Yamaguchi and S. Koda, J. Chem. Phys. **132**, 114502 (2010).
[16] J.-P. Hansen and I. R. McDonald, *Theory of Simple Liquids*, 2nd ed. (Academic Press, London, 1986).
[17] J.-P. Boon and S. Yip, *Molecular Hydrodynamics* (Dover Publications, New York, 1991).
[18] U. Balucani and M. Zoppi, *Dynamics of the Liquid State* (Clarendon Press, Oxford, 1994).
[19] F. Hirata, *Molecular Theory of Solvation* (Kluwer, Dordrecht, 2003).
[20] S.-H. Chong, W. Götze, and A. P. Singh, Phys. Rev. E **63**, 011206 (2000).
[21] T. Yamaguchi, K. Mikawa, S. Koda, K. Fujii, H. Endo, M. Shibayama, H. Hamano, and Y. Umebayashi, J. Chem. Phys. **137**, 104511 (2012).
[22] T. Yamaguchi, T. Yonezawa, and S. Koda, Phys. Chem. Chem. Phys. **17**, 19126 (2015).
[23] T. Imae, T. Kanaya, M. Furusaka, and N. Torikai, *Neutron in Soft Matter* (Wiley, Hoboken, 2011).
[24] T. Yamaguchi, T. Matsuoka, and S. Koda, J. Chem. Phys. **122**, 014512 (2005).
[25] T. Yamaguchi, T. Matsuoka, and S. Koda, J. Mol. Liq. **134**, 1 (2007).
[26] T. Yamaguchi, T. Matsuoka, and S. Koda, J. Chem. Phys. **126**, 144505 (2007).
[27] T. Yamaguchi, T. Matsuoka, and S. Koda, J. Chem. Phys. **127**, 234501 (2007).
[28] M. J. Abraham, T. Murtola, R. Schulz, S. Pall, J. C. Smith, B. Hess, and E. Lindahl, SoftwareX **1**, 19 (2015).
[29] The identification of any commercial product or trade name does not imply endorsement or recommendation by the National Institute of Standards and Technology.
[30] W. L. Jorgensen, D. S. Maxwell, and J. Tirado-Rives, J. Am. Chem. Soc. **118**, 11225 (1996).
[31] M. P. Allen and D. J. Tildesley, *Computer Simulation of Liquids* (Clarendon Press, Oxford, 1987).
[32] B. Hess, H. Bekker, H. J. C. Berendsen, and J. G. E. M. Fraaije, J. Comput. Chem. **18**, 1463 (1997).
[33] J. A. Riddick, W. B. Bunger, and T. K. Sakano, *Organic Solvents*, 4th ed. (John Wiley & Sons, New York, 1986).
[34] T. Yamaguchi, J. Chem. Phys. **144**, 124514 (2016).
[35] J. Wu, Y. Liu, W.-R. Chen, J. Cao, and S.-H. Chen, Phys. Rev. E **70**, 050401(R) (2004).
[36] O. Henrich, A. M. Puertas, M. Sperl, J. Baschnagel, and M. Fuchs, Phys. Rev. E **76**, 031404 (2007).